(Received 6 October 2023, Accepted 27 November 2023, Scheduled 8 December 2023)

Generalized Phase Retrieval Model based on Physics-Inspired Network for Holographic Metasurface

Lei Jin*, Jialei Xie, Baicao Pan, and Guoqing Luo

Key Laboratory of RF Circuits & System of Ministry of Education, School of Electronics and Information Hangzhou Dianzi University, Xiasha High Education Park, Hangzhou 310018, China

ABSTRACT: Phase holographic metasurfaces encode the phase profiles of holograms in metasurfaces formed by meta-atom arrays and accurately modulate the field distribution in desired region. Iterative optimization methods or data-driven learning methods are used to retrieve the phase profile under the given physical setups, such as working wavelength λ, metasurfaces' period Δx, and image distance Z. However, those methods usually repeat the optimization or training process to retrieve the phase profile for different physical setups. Here, we propose a generalized phase retrieval model (GPRM) based on physics-inspired network to retrieve the phase profile from the input λ, Δx, Z, and desired image without retraining the neural network. The GPRM consists of deep neural network (DNN), parabolic phase, and Fresnel diffraction propagation, which is able to generate phase profile with high reconstruction quality in extraordinary broadband, such as visible, terahertz, and microwave region. By combining with corresponding meta-atom pool, the proposed method has great potential to design versatile meta-devices for image display, data encoding, and beam shaping. Furthermore, the proposed method accelerates the design of Fresnel phase hologram, which can cooperate with programmable metasurfaces to realize dynamic three-dimensional or full-color display.

1. INTRODUCTION

Metasurfaces formed by a 2-dimensional array of engineered meta-atom have extraordinary capabilities to operate electromagnetic wave in subwavelength scale [1–4]. Based on the interaction between the incident electromagnetic wave and tailoring meta-atoms, metasurfaces are able to locally control the amplitude [5, 6], phase [7, 8], and polarization [8–10] of incident wave. Due to the extraordinary capabilities, metasurfaces have attracted significant attention and been exploited to realize a variety of functionalities, such as quantum light source [11], thermally emitted light [12], unidirectional propagation [13], spectropolarimeter [14], biosensing [15], bioimaging [16], image processing [17], and hologram [18].

Those remarkable functionalities are dependent on the flexibility in designing meta-atoms and their arrangements. To accurately control incident wave in subwavelength scale, the geometry and subwavelength period Δx of meta-atom are often designed by full-wave simulation collaborating with parameter sweep [9] or optimization methods [19]. The designed meta-atoms are required to arrange in a certain way to manipulate the wavefront. For given meta-atoms, the arrangement affects the quality of wavefront manipulation [20] and the performance of metasurface [21, 22]. For example, in our previous works, it is demonstrated that by designing the arrangement, the metasurfaces with single-size nanobrick arrays are able to realize multi-momentum transformation [23] and carry massive information on 6-bit encode color holograms [24]. Therefore, achieving a suitable arrangement is a critical part of metasurface design.

The computer generation holography (CGH) is an important approach for designing the arrangement of meta-atoms. CGH retrieves the hologram with phase or amplitude distribution to reconstruct the desired filed distribution in three-dimensional space [25]. The retrieved hologram is encoded into the holographic metasurface by arranging the meta-atoms. Because the phase-only hologram provides higher working efficiency than the amplitude hologram, most of holographic metasurfaces carry the phase profile (i.e., the phase distribution) of phase-only hologram, and the value of phase is in the range of $[-\pi, \pi]$. As shown in Fig. 1(a), the phase profile is required to be designed under the given metasurface's period Δx, working wavelength λ, distance Z, and desired field distribution, which is a typical phase retrieval problem [26–28]. To retrieve the phase profiles under the given conditions, iterative algorithms, such as Gerchberg-Saxton (GS) algorithm [23, 24, 29, 30], are often employed. For different given conditions, those methods usually repeat the iterative optimization process to retrieve the phase profiles, which is time consuming. To reduce the optimization time, deep learning algorithm is exploited to generate the phase profile of hologram after off-line training process and has great potential to realize real-time retrieval with high performance using the trained networks [31–35]. However, the trained network is usually suitable for the fixed working wavelength λ, period Δx, or the distance Z used in the training process. In other words, if the above physical setups are changed,

* Corresponding author: Lei Jin (elejinlei@hdu.edu.cn).

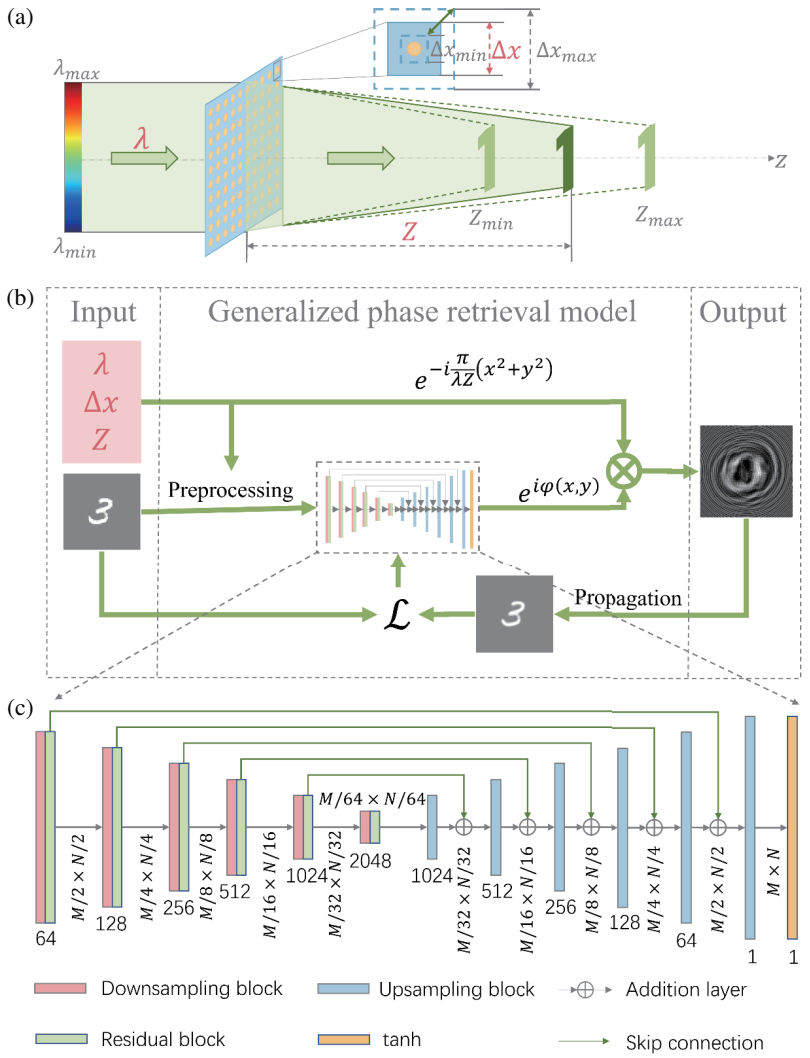

FIGURE 1. (a) Schematic of holographic metasurface. λ is the working wavelength. Δx is the metasurface's period. Z is the distance between the metasurface plane and image plane. (b) Architecture of generalized phase retrieval model (GPRM) to retrieve Fresnel hologram (output) from the given λ, Δx, Z, and desired image (input). (c) Architecture of U-Net in GPRM.

it is required to re-accumulate training data and retraining the network, which costs a lot of time.

To retrieve the phase profile of metasurface at different physical setups, this paper proposes a generalized phase retrieval model (GPRM) based on physics-inspired network. The GPRM formed by U-net [36–38], parabolic phase, and Fresnel diffraction propagation is an unsupervised neural network, and has the capability to retrieve the phase profile from the input λ, Δx, Z, and desired image. U-net is used to design the Fourier hologram of input desired image. The parabolic phase converts the Fourier hologram to Fresnel hologram, and the reconstructed image can be achieved by Fresnel diffraction propagation. Due to the incorporating of physical prior knowledge, the GPRM trained in the visible region achieves nice reconstruction quality at different bands, such as terahertz and microwave region. It is expected that the proposed method can be further extended to design versatile meta-devices for real-time image display, data encoding, and beam shaping.

2. PRINCIPLE

2.1. Theory

Holographic metasurface encodes the information of hologram in metasurfaces, where a metasurface is formed by meta-atom array with subwavelength period Δx. To realize phase-only hologram, the phase distribution of hologram is encoded in holographic metasurface as its phase profile, and the value of phase is in the range of $[-\pi, \pi]$. As shown in Fig. 1(a), when a monochromatic beam with wavelength λ illuminates the metasurface, this beam carries phase profile of the metasurface and reconstructs a complex field distribution at image plane. The distance between metasurface and image planes is Z, and the complex field distribution is expressed by Fresnel diffraction [39]:

$$U_2(x_2, y_2, Z) = \frac{e^{ikZ}}{i\lambda Z} e^{i\frac{k}{2Z}(x_2^2+y_2^2)} \iint_{-\infty}^{+\infty}$$

$$\left\{e^{i\psi(x_1,y_1)}e^{i\frac{k}{2Z}\left(x_1^2+y_1^2\right)}\right\}e^{-i\frac{2\pi}{\lambda Z}(x_1x_2+y_1y_2)}dx_1dy_1 \quad (1)$$

where (x_1, y_1) and (x_2, y_2) are the spatial coordinates at the metasurface and image planes, respectively. Here, k is the wavenumber, $\psi(x_1, y_1)$ the phase profile carried by metasurface, and $e^{i\psi(x_1,y_1)}$ the Fresnel hologram of the product of the desired image. Therefore, to design the phase profile of holographic metasurface, metasurface's period Δx, working wavelength λ, and the distance Z are required. To find the relationship among Δx, λ, and Z, the metasurface's phase profile $\psi(x_1, y_1)$ is divided into two parts [40] in the form of

$$e^{i\psi(x_1,y_1)} = e^{i\varphi(x_1,y_1)}e^{-i\frac{\pi}{\lambda Z}\left(x_1^2+y_1^2\right)}, \quad (2)$$

and the complex field distribution in Eq. (1) is rewritten as

$$U_2(x_2,y_2,Z) = \frac{e^{ikZ}}{i\lambda Z}e^{i\frac{k}{2Z}\left(x_2^2+y_2^2\right)} \iint_{-\infty}^{+\infty} e^{i\varphi(x_1,y_1)}e^{-i\frac{2\pi}{\lambda Z}(x_1x_2+y_1y_2)}dx_1dy_1 \quad (3)$$

where the Fresnel diffraction is reduced to a Fraunhofer diffraction [39] at the image plane, and $e^{i\varphi(x_1,y_1)}$ is the Fourier hologram of the product of the desired image. According to Eq. (3), when Δx, λ, and Z are chosen from different regions ($[\Delta x_{\min}, \Delta x_{\max}]$, $[\lambda_{\min}, \lambda_{\max}]$, $[Z_{\min}, Z_{\max}]$) and $\Delta x^2/(\lambda Z)$ equal to a constant, the designed Fourier hologram $e^{i\varphi}$ will achieve the same matrix of intensity distribution.

2.2. Network Architecture

To realize the general model for inversely designing Fresnel holographic metasurface, an unsupervised neural network driven by a physics-based model is proposed and shown in Fig. 1(b). This model is used to retrieve phase profile ($N \times N$ pixels) of Fresnel hologram (output) from the given λ, Δx, Z, and desired image (input). According to Eq. (2), the phase profile of Fresnel meta-hologram is divided into two parts: parabolic phase $e^{-i\frac{\pi}{\lambda Z}\left(x_1^2+y_1^2\right)}$ and Fourier hologram $e^{i\varphi(x_1,y_1)}$. The inputs λ, Δx, and Z are used to calculate the parabolic phase $e^{-i\frac{\pi}{\lambda Z}\left(x_1^2+y_1^2\right)}$ and preprocess the input image. The preprocessing resizes the input images to offset the magnification or minification of reconstructed image. The width of the resized image is proportional to $\Delta x/(\lambda Z)$. The resized image is the input of U-Net for Fourier hologram $e^{i\varphi(x_1,y_1)}$ generation. The Fresnel meta-hologram (output) is obtained by multiplying the parabolic phase $e^{-i\frac{\pi}{\lambda Z}\left(x_1^2+y_1^2\right)}$ and Fourier hologram $e^{i\varphi(x_1,y_1)}$. The Fresnel diffraction propagation function is employed to calculate the reconstructed image at the image plane. The loss function $\mathcal{L}$ calculates the error between the reconstructed image and the input image to update the parameters of U-net. Here, the loss function is mean square error (MSE) [41]:

$$MSE = \frac{1}{mn}\sum_{p=1}^{m}\sum_{q=1}^{n}\left|I(x_p,y_q) - I_0(x_p,y_q)\right|^2 \quad (4)$$

where $I_0(x, y)$ represents the input image. $I(x, y) = |U_2(x, y, z)|^2$ represents the reconstructed image, and U_2 is the complex field distribution in Eq. (3).

Fresnel impulse response propagator (FIRP) [42] is used to calculate the Fresnel diffraction propagation function:

$$U_2(x,y,z) = \Im^{-1}\left\{\Im\left\{e^{i\varphi(x,y)}e^{-i\frac{\pi}{\lambda z}\left(x^2+y^2\right)}\right\}\Im\{h(x,y,z)\}\right\} \quad (5)$$

where $\Im$ and $\Im^{-1}$ are Fourier transform and inverse Fourier transform, respectively. h is the impulse response:

$$h(x,y,z) = \frac{e^{ikz}}{i\lambda z}e^{i\frac{k}{2z}\left(x^2+y^2\right)} \quad (6)$$

3. RESULTS

The PyTorch deep learning framework is utilized to construct GPRM. All the algorithms are run on the same workstation equipped with an Intel Xeon Platinum 8352Y CPU and an NVIDIA GeForce RTX 3080 GPU. The images of handwritten digits (Modified National Institute of standards and technology (MNIST) database) are used to train and test GPRM. 5000 images are involved to train the model, and another 2000 images are used to test the model's performance. The training epoch is set as 500, and the training time is 4.5 hours. In the training process, the sizes of input image and output phase profile are fixed at 256×256 pixels. The metasurface's period Δx is 300 nm, and wavelength λ is in the visible region [400 nm, 800 nm]. According to the sampling theorem, the distance z is chosen in the region [115.2 μm, 230.4 μm]. Therefore, the value of $\Delta x^2/(\lambda Z)$ is chosen in the region $\left[0.4\times10^{-3}, 2\times10^{-3}\right]$ during the training process.

After the training process, the GPRM with optimized parameters has the capability to rapidly retrieve the phase profile of holographic metasurface. Test results for each part of GPRM are shown in Fig. 2. Based on the inputting physical setups ($\lambda = 600$ nm, $\Delta x = 300$ nm, and $Z = 115.2$ μm), GPRM resizes the image from Fig. 2(b)① to Fig. 2(b)②, and the width of resized image is proportional to $\Delta x/(\lambda Z)$. The resized image is input into the U-net to achieve the Fourier hologram $e^{i\varphi(x,y)}$. The phase profile of Fourier hologram and corresponding reconstructed image are presented in Fig. 2(b)③ and ④, respectively. Note that the image ④ is reconstructed at Fraunhofer domain (k-space) via Fraunhofer propagator (FP). By multiplying the parabolic phase $e^{-i\frac{\pi}{\lambda Z}\left(x^2+y^2\right)}$ and Fourier hologram $e^{i\varphi(x,y)}$, the phase profile of Fresnel hologram (shown in Fig. 2(b)⑤) is achieved and reconstructs image (Fig. 2(b)⑥) at given image plane. Comparing Fig. 2(b)① and ⑥, the reconstructed image has the same size as the input image and restores the features of input image nicely.

To evaluate the performance of the GPRM, the GS algorithm is also used to retrieve the phase profile as shown in Fig. 3. The GPRM only takes 0.014 s and is faster than GS algorithm. The peak signal-to-noise ratio (PSNR) and structural similarity

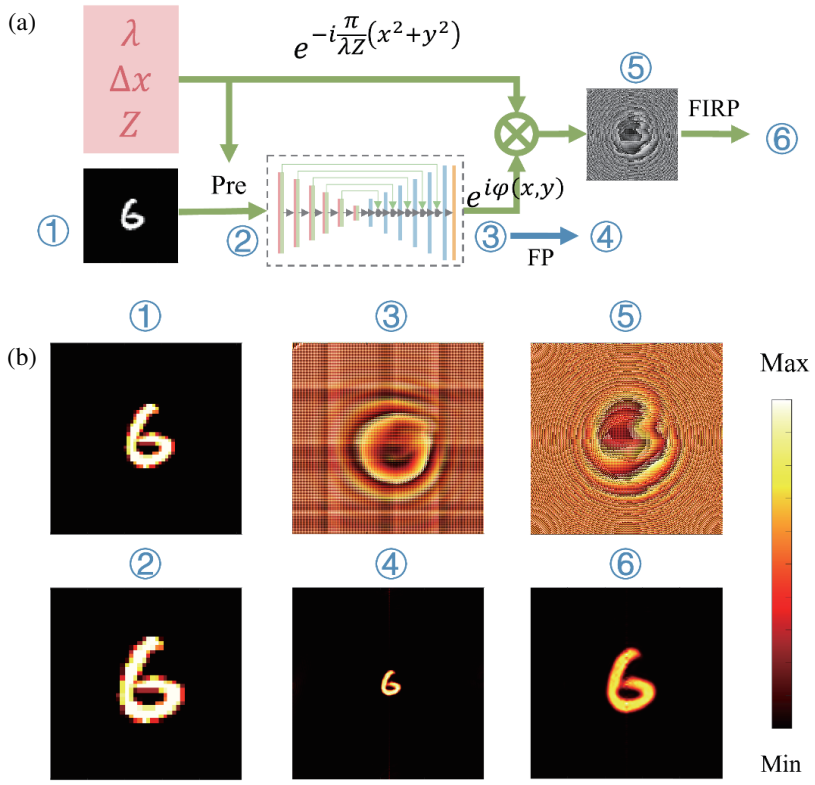

FIGURE 2. (a) Schematic of retrieving the phase profile of holographic metasurface via trained GPRM. Pre: preprocessing; FP: Fraunhofer propagator; FIRP: Fresnel impulse response propagator. (b) Test results for each part of GPRM. ①: Input image; ②: Preprocessed Image; ③: Phase profile of Fourier hologram; ④: Reconstructed image of Fourier hologram at Fraunhofer domain; ⑤: Phase profile of Fresnel hologram (output) ⑥: Reconstructed image of output at Fresnel domain.

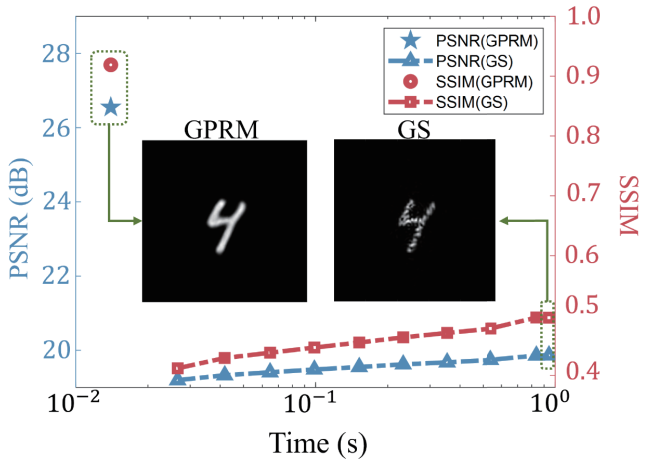

FIGURE 3. Evaluation the running time and reconstruction quality of GPRM and GS algorithm. PSNR: peak signal-to-noise ratio. SSIM: structural similarity index measure. Inset: reconstructed image for GPRM and GS algorithm.

index measure (SSIM) are employed to evaluate the quality of reconstructed image. The expressions of PSNR and SSIM are

$$PSNR = 10\log_{10}\left(\frac{I_{\max}^2}{MSE}\right) \tag{7}$$

$$SSIM = \frac{(2u_iu_r + c_1)(2\sigma_{ir} + c_2)}{(u_i^2 + u_r^2 + c_1)(\sigma_i^2 + \sigma_r^2 + c_2)} \tag{8}$$

where $I_{\max}$ is the maximum intensity of image, and u_i and u_r are the mean of input and reconstructed images, respectively. σ_i^2 and σ_r^2 are the variance, and σ_{ir} is the covariance. c_1 and c_2 are a structural constant. Figure 3 shows the average PSNR and SSIM of 100 samples. As shown in Fig. 3, the GPRM achieves higher PSNR and SSIM than GS algorithm. According to the

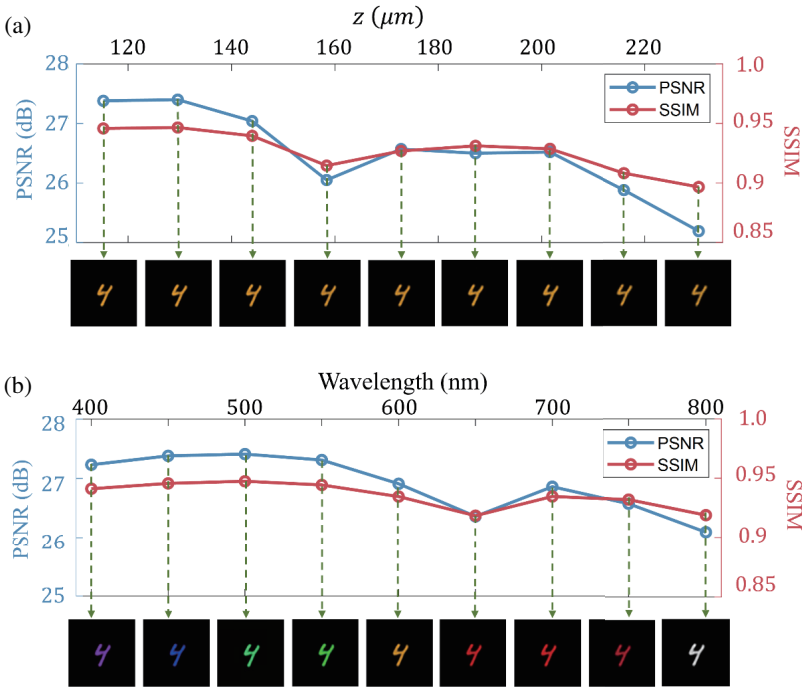

FIGURE 4. (a) The reconstruction quality for a given wavelength at different image distances. (b) The reconstruction quality for different wavelengths at a given image distance.

inset of Fig. 3, the image reconstructed by GPRM has uniform field distribution suppressed the sparkle noise.

The GPRM has the capability to retrieve the phase profile for different wavelengths at different image distances. Figure 4(a) shows the reconstructed images for a given wavelength 600 nm in an image distance region [115.2 μm, 230.4 μm]. These reconstructed images have uniform field distribution and restore the features of designed image nicely. The average PSNR and SSIM are 26.5 dB and 0.92, respectively. Figure 4(b) presents the reconstructed images at a fixed image distance in a wavelength region [400 nm, 800 nm]. The GPRM achieves high fidelity reconstruction with 26.9 dB PSNR and 0.93 SSIM.

4. DISCUSSION

According to Eqs. (5) and (6), the reconstructed field is expressed by the Fourier hologram $e^{i\varphi}$, parabolic phase $e^{-i\frac{\pi}{\lambda z}\left(x^2+y^2\right)}$, and impulse response h. The phase matrix of Fourier hologram $e^{i\varphi}$ designed by U-net is independent of metasurface's period Δx, working wavelength λ and the distance Z. Δx, λ, and Z affect the calculation of the parabolic phase and impulse response, and the expression of these two parts is involved in GPRM. Therefore, the proposed GPRM has the capability to achieve high reconstruction quality for different wavelengths at different image distances. According to Eq. (3), when $\Delta x^2/(\lambda z)$ equals a constant, the designed Fourier hologram $e^{i\varphi}$ will achieve the same intensity distribution. Based on this dispersion relation, the effect of metasurface's period Δx can be solved by changing working wavelength λ and distance Z.

The phase profile retrieved by GPRM is encoded in the metasurface by arranging meta-atoms. As shown in Fig. 1(a), the collimated laser beam normally illuminates the metasurface, carries the phase profile, and reconstructs desired image at the image plane. Because of the subwavelength pixel size, an objective lens is required to collect the reconstructed image before the captured plane of the charge-coupled device (CCD) camera. Moreover, Fig. 1(a) shows that the proposed GPRM retrieves the phase profile for the on-axis system, while this method could extend to off-axis system by adding appropriate gradient phase.

Although this model is trained in the visible region, the proposed GPRM is able to be directly applied to other bands, such as terahertz wave and microwave. If λ, Δx, and Z are enlarged by N times at the same time, the value of $(N\Delta x)^2/(N\lambda \times NZ)$ will be unchanged, which leads to the same matrix of intensity distribution. As shown in Fig. 5, the GPRM achieves nice reconstruction quality at different bands. The restricted condition is that the inputs of the GPRM (i.e., λ, Δx, and Z) are required to satisfy the value of $\Delta x^2/(\lambda Z)$ used in the training data. The value of $\Delta x^2/(\lambda Z)$ is limited by the sampling theorem of Fresnel propagator. By employing different Fresnel propagation approaches [42], the GPRM has the capability to broaden the range of application.

The reconstruction quality is dependent on the network frameworks. To analyze the effect of network framework, the U-Net architectures in the GPRM are designed to contain 4 and 5 sampling (downsampling and upsampling) layers. 2000 images are used to test their performance, which is presented in Fig. 6. By increasing the number of sampling layers in U-net,

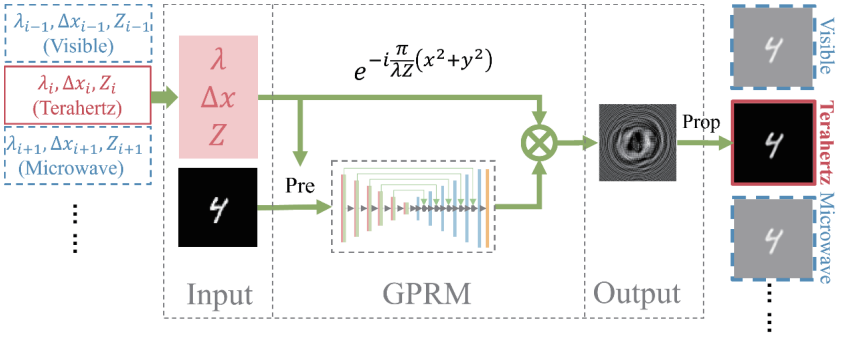

FIGURE 5. GPRM directly retrieves the holographic phase profile in full band, such as visible wave, terahertz wave, and microwave. Pre: preprocessing; Prop: Fresnel propagation.

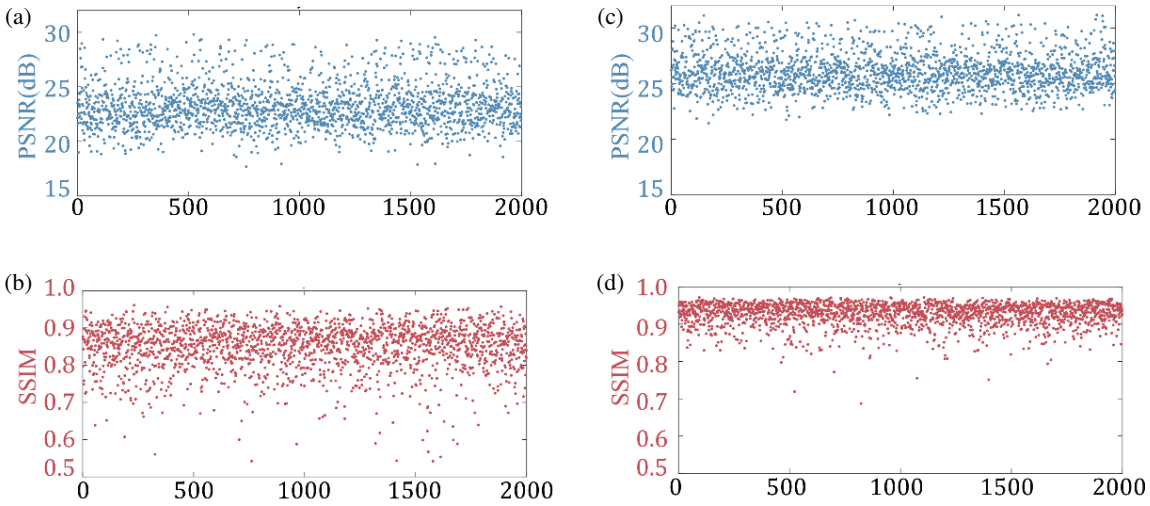

FIGURE 6. The reconstructed quality of GPRM including 4 (a), (b) and 5 (c), (d) sampling layers. PSNR (a), (c) and SSIM (b), (d) for the 2000 testing images.

the average PSNR and SSIM are increased from 23.26 dB and 0.84 to 26.00 dB and 0.92, respectively. Therefore, the reconstruction quality can be significantly improved by enhancing the learning capability of U-net.

5. CONCLUSION

In this paper, GPRM is proposed to retrieve the phase profile from the input λ, Δx, Z, and desired image. This model is trained in the visible region. After training process, the GPRM only takes 0.014 s to achieve the phase profile, and the reconstruct images have uniform intensity distribution, 26.5 dB average PSNR and 0.92 average SSIM. Moreover, the proposed GPRM is able to directly applied to another band. By changing the propagator, the applicable range of GPRM will be further extended. The proposed method involving different λ and Z also has a great potential to apply to multi-plane holography and full-color holography.

ACKNOWLEDGEMENT

L. Jin acknowledges National Natural Science Foundation of China (NSFC) (Contract 62105084) and Natural Science Foundation of Zhejiang Province (Contract LQ22F050019). G. Q. Luo acknowledges National Natural Science Foundation of China (NSFC) (Contract 62125105).

Data availability: Data underlying the results presented in this paper can be obtained from the authors upon reasonable request.

Disclosures: The authors declare no conflicts of interest.

REFERENCES

[1] Yu, N., P. Genevet, M. A. Kats, F. Aieta, J.-P. Tetienne, F. Capasso, and Z. Gaburro, "Light propagation with phase discontinuities: Generalized laws of reflection and refraction," *Science*, Vol. 334, No. 6054, 333–337, Oct. 2011.

[2] Qiu, C.-W., T. Zhang, G. Hu, and Y. Kivshar, "Quo vadis, metasurfaces?" *Nano Letters*, Vol. 21, No. 13, 5461–5474, 2021.

[3] Wu, N., Y. Zhang, H. Ma, H. Chen, and H. Qian, "Tunable high-Q plasmonic metasurface with multiple surface lattice res-

onances," *Progress In Electromagnetics Research*, Vol. 172, 23–32, 2021.

[4] Li, L., H. Zhao, C. Liu, L. Li, and T. J. Cui, "Intelligent metasurfaces: control, communication and computing," *Elight*, Vol. 2, No. 1, 2022.

[5] Dong, Z., J. Ho, Y. F. Yu, Y. H. Fu, R. Paniagua-Dominguez, S. Wang, A. I. Kuznetsov, and J. K. W. Yang, "Printing beyond sRGB color gamut by mimicking silicon nanostructures in free-space," *Nano Letters*, Vol. 17, No. 12, 7620–7628, Dec. 2017.

[6] Song, M., L. Feng, P. Huo, M. Liu, C. Huang, F. Yan, Y.-Q. Lu, and T. Xu, "Versatile full-colour nanopainting enabled by a pixelated plasmonic metasurface," *Nature Nanotechnology*, Vol. 18, No. 1, 71, Jan. 2023.

[7] Huang, L., X. Chen, H. Muehlenbernd, G. Li, B. Bai, Q. Tan, G. Jin, T. Zentgraf, and S. Zhang, "Dispersionless phase discontinuities for controlling light propagation," *Nano Letters*, Vol. 12, No. 11, 5750–5755, Nov. 2012.

[8] Liu, M., W. Zhu, P. Huo, L. Feng, M. Song, C. Zhang, L. Chen, H. J. Lezec, Y. Lu, A. Agrawal, and T. Xu, "Multifunctional metasurfaces enabled by simultaneous and independent control of phase and amplitude for orthogonal polarization states," *Light-science & Applications*, Vol. 10, No. 1, May 2021.

[9] Yang, H., Y. Jiang, Y. Hu, K. Ou, and H. Duan, "Noninterleaved metasurface for full-polarization three-dimensional vectorial holography," *Laser & Photonics Reviews*, Vol. 16, No. 11, Nov. 2022.

[10] Wu, P. C., W.-Y. Tsai, W. T. Chen, Y.-W. Huang, T.-Y. Chen, J.-W. Chen, C. Y. Liao, C. H. Chu, G. Sun, and D. P. Tsai, "Versatile polarization generation with an aluminum plasmonic metasurface," *Nano Letters*, Vol. 17, No. 1, 445–452, Jan. 2017.

[11] Li, L., Z. Liu, X. Ren, S. Wang, V.-C. Su, M.-K. Chen, C. H. Chu, H. Y. Kuo, B. Liu, W. Zang, G. Guo, L. Zhang, Z. Wang, S. Zhu, and D. P. Tsai, "Metalens-array-based high-dimensional and multiphoton quantum source," *Science*, Vol. 368, No. 6498, 1487, Jun. 2020.

[12] Overvig, A. C., S. A. Mann, and A. Alu, "Thermal metasurfaces: complete emission control by combining local and nonlocal light-matter interactions," *Physical Review X*, Vol. 11, No. 2, Jun. 2021.

[13] Li, Z., G. Cao, C. Li, S. Dong, Y. Deng, X. Liu, J. S. Ho, and C.-W. Qiu, "Non-hermitian electromagnetic metasurfaces at exceptional points," *Progress In Electromagnetics Research*, Vol. 171, 1–20, 2021.

[14] Ni, Y., C. Chen, S. Wen, X. Xue, L. Sun, and Y. Yang, "Computational spectropolarimetry with a tunable liquid crystal metasurface," *Elight*, Vol. 2, No. 1, Nov. 2022.

[15] Tittl, A., A. Leitis, M. Liu, F. Yesilkoy, D.-Y. Choi, D. N. Neshev, Y. S. Kivshar, and H. Altug, "Imaging-based molecular barcoding with pixelated dielectric metasurfaces," *Science*, Vol. 360, No. 6393, 1105, Jun. 2018.

[16] Pahlevaninezhad, H., M. Khorasaninejad, Y.-W. Huang, Z. Shi, L. P. Hariri, D. C. Adams, V. Ding, A. Zhu, C.-W. Qiu, F. Capasso, and M. J. Suter, "Nano-optic endoscope for high-resolution optical coherence tomography in vivo," *Nature Photonics*, Vol. 12, No. 9, 540, Sep. 2018.

[17] Cordaro, A., H. Kwon, D. Sounas, A. F. Koenderink, A. Alu, and A. Polman, "High-index dielectric metasurfaces performing mathematical operations," *Nano Letters*, Vol. 19, No. 12, 8148–8423, Dec. 2019.

[18] Huang, L., S. Zhang, and T. Zentgraf, "Metasurface holography: From fundamentals to applications," *Nanophotonics*, Vol. 7, No. 6, SI, 1169–1190, Jun. 2018.

[19] Dong, Z., L. Jin, S. D. Rezaei, H. Wang, Y. Chen, F. Tjiptoharsono, J. Ho, S. Gorelik, R. J. H. Ng, Q. Ruan, C.-W. Qiu, and J. K. W. Yang, "Schrodinger's red pixel by quasi-bound-states-in-the-continuum," *Science Advances*, Vol. 8, No. 8, Feb. 2022.

[20] Huang, K., H. Liu, F. J. Garcia-Vidal, M. Hong, B. Luk'yanchuk, J. Teng, and C.-W. Qiu, "Ultrahigh-capacity non-periodic photon sieves operating in visible light," *Nature Communications*, Vol. 6, May 2015.

[21] Ren, H., X. Fang, J. Jang, J. Buerger, J. Rho, and S. A. Maier, "Complex-amplitude metasurface-based orbital angular momentum holography in momentum space," *Nature Nanotechnology*, Vol. 15, No. 11, 948, Nov. 2020.

[22] Li, C., J. Jang, T. Badloe, T. Yang, J. Kim, J. Kim, M. Nguyen, S. A. Maier, J. Rho, H. Ren *et al.*, "Arbitrarily structured quantum emission with a multifunctional metalens," *Elight*, Vol. 3, No. 1, 19, 2023.

[23] Jin, L., Y.-W. Huang, Z. Jin, R. C. Devlin, Z. Dong, S. Mei, M. Jiang, W. T. Chen, Z. Wei, H. Liu, J. Teng, A. Danner, X. Li, S. Xiao, S. Zhang, C. Yu, J. K. W. Yang, F. Capasso, and C.-W. Qiu, "Dielectric multi-momentum meta-transformer in the visible," *Nature Communications*, Vol. 10, Oct. 2019.

[24] Jin, L., Z. Dong, S. Mei, Y. F. Yu, Z. Wei, Z. Pan, S. D. Rezaei, X. Li, A. I. Kuznetsov, Y. S. Kivshar, J. K. W. Yang, and C.-W. Qiu, "Noninterleaved metasurface for (2^6-1) spin- and wavelength-encoded holograms," *Nano Letters*, Vol. 18, No. 12, 8016–8024, Dec. 2018.

[25] Javidi, B., A. Carnicer, A. Anand, G. Barbastathis, W. Chen, P. Ferraro, J. W. Goodman, R. Horisaki, K. Khare, M. Kujawinska, R. A. Leitgeb, P. Marquet, T. Nomura, A. Ozcan, Y. Park, G. Pedrini, P. Picart, J. Rosen, G. Saavedra, N. T. Shaked, A. Stern, E. Tajahuerce, L. Tian, G. Wetzstein, and M. Yamaguchi, "Roadmap on digital holography," *Optics Express*, Vol. 29, No. 22, 35 078–35 118, Oct. 2021.

[26] Zhang, D., Y. Guo, F. Sun, and H. Liu, "Unique determinations in inverse scattering problems with phaseless near-field measurements," *Inverse Problems and Imaging*, Vol. 14, No. 3, 569–582, Jun. 2020.

[27] Zhang, D., Y. Guo, J. Li, and H. Liu, "Retrieval of acoustic sources from multi-frequency phaseless data," *Inverse Problems*, Vol. 34, No. 9, Sep. 2018.

[28] Yin, W., W. Yang, and H. Liu, "A neural network scheme for recovering scattering obstacles with limited phaseless far-field data," *Journal of Computational Physics*, Vol. 417, Sep. 2020.

[29] Gerchberg, R. W. and W. O. Saxton, "A practical algorithm for the determination of plane from image and diffraction pictures," *Optik*, Vol. 35, No. 2, 237–246, 1972.

[30] Ma, W., Y. Xu, B. Xiong, L. Deng, R.-W. Peng, M. Wang, and Y. Liu, "Pushing the limits of functionality-multiplexing capability in metasurface design based on statistical machine learning," *Advanced Materials*, Vol. 34, No. 16, Apr. 2022.

[31] Shimobaba, T., D. Blinder, T. Birnbaum, I. Hoshi, H. Shiomi, P. Schelkens, and T. Ito, "Deep-learning computational holography: A review," *Frontiers in Photonics*, Vol. 3, 2022.

[32] Liu, K., J. Wu, Z. He, and L. Cao, "4K-dmdnet: diffraction model-driven network for 4K computer-generated holography," *Opto-electronic Advances*, Vol. 6, No. 5, 2023.

[33] Zou, Y., R. Zhu, L. Shen, and B. Zheng, "Reconfigurable metasurface hologram of dynamic distance via deep learning," *Frontiers in Materials*, Vol. 9, 220 135–1–220 135–13., May 2022.

[34] Li, R., G. Pedrini, Z. Huang, S. Reichelt, and L. Cao, "Physics-enhanced neural network for phase retrieval from two diffraction patterns," *Optics Express*, Vol. 30, No. 18, 32 680–32 692, Aug. 2022.

[35] Peng, Y., S. Choi, N. Padmanaban, J. Kim, and G. Wetzstein, "Neural holography," in *ACM Siggraph 2020 Emerging Technologies*, Electr Network, Aug 2020.

[36] Ronneberger, O., P. Fischer, and T. Brox, "U-net: convolutional networks for biomedical image segmentation," in *Medical Image Computing and Computer-assisted Intervention, Pt Iii*, Vol. 9351, 234–241, Munich, Germany, Oct. 2015.

[37] Wei, Z. and X. Chen, "Physics-inspired convolutional neural network for solving full-wave inverse scattering problems," *IEEE Transactions on Antennas and Propagation*, Vol. 67, No. 9, 6138–6148, Sep. 2019.

[38] Gong, D., T. Ma, J. Evans, and S. He, "Deep neural networks for image super-resolution in optical microscopy by using modified hybrid task cascade u-net," *Progress In Electromagnetics Research*, Vol. 171, 185–199, 2021.

[39] Goodman, J. W., *Introduction to Fourier Optics*, Roberts and Company Publishers, 2005.

[40] Makey, G., O. Yavuz, D. K. Kesim, A. Turnali, P. Elahi, S. Ilday, O. Tokel, and F. O. Ilday, "Breaking crosstalk limits to dynamic holography using orthogonality of high-dimensional random vectors," *Nature Photonics*, Vol. 13, No. 4, 251, Apr. 2019.

[41] Zhang, Y., M. Zhang, K. Liu, Z. He, and L. Cao, "Progress of the computer-generated holography based on deep learning," *Applied Sciences*, Vol. 12, No. 17, Sep. 2022.

[42] Voelz, D. G. and M. C. Roggemann, "Digital simulation of scalar optical diffraction: revisiting chirp function sampling criteria and consequences," *Applied Optics*, Vol. 48, No. 32, 6132–6142, Nov. 2009.